Inorganic Chemistry

Article

pubs.acs.org/IC

# Conformation-Controlled Sorption Properties and Breathing of the Aliphatic Al-MOF [Al(OH)(CDC)]

Felicitas Niekiel,[†] Jeroen Lannoeye,[‡] Helge Reinsch,[‡] Alexis S. Munn,[§] Andreas Heerwig,[∥] Ivo Zizak,[⊥] Stefan Kaskel,[∥] Richard I. Walton,[§] Dirk de Vos,[‡] Philip Llewellyn,[#] Alexandra Lieb,[¶] Guillaume Maurin,*[,▽] and Norbert Stock*[,†]

[†]Institut für Anorganische Chemie, Christian-Albrechts-Universität zu Kiel, Max-Eyth-Straße 2, 24118 Kiel, Germany

[‡]Centre for Surface Chemistry and Catalysis, Katholieke Universiteit Leuven, Arenbergpark 23, B-3001 Leuven, Belgium

[§]Department of Chemistry, University of Warwick, Coventry CV4 7AL, United Kingdom

[∥]Department of Inorganic Chemistry, Dresden University of Technology, Bergstraße 66, 01069 Dresden, Germany

[⊥]Institute of Nanometer Optics and Technology, Helmholtz Zentrum Berlin für Materialien und Energie, Albert-Einstein-Straße 15, 12489 Berlin, Germany

[#]Aix-Marseille Université, CNRS, Laboratoire MADIREL (UMR7246), Centre de Saint Jérôme, 13397 Marseille Cedex 2, France

[¶]Institut für Chemie, Otto-von-Guericke-Universität Magdeburg, Universitätsplatz 2, 39106 Magdeburg, Germany

[▽]Institut Charles Gerhardt Montpellier, UMR CNRS 5253, UM2, ENSCM, Place E. Bataillon, 34095 Montpellier Cedex 05, France

Supporting Information

**ABSTRACT:** The Al-MOF CAU-13 ([Al(OH)(*trans*-CDC)]; *trans*-$H_2$CDC = *trans*-1,4-cyclohexanedicarboxylic acid) is structurally related to the MIL-53 compounds that are well-known for their "breathing" behavior, i.e., the framework flexibility upon external stimuli such as the presence of adsorbate molecules. The adsorption properties of CAU-13 were investigated in detail. The sorption isotherms of $N_2$, $H_2$, $CH_4$, CO, $CO_2$, and water were recorded, and the adsorption enthalpies for the gases were determined by microcalorimetry. The structural changes upon adsorption of $CO_2$ were followed with in situ synchrotron powder X-ray diffraction (PXRD). The patterns were analyzed by parametric unit cell refinement, and the preferential arrangement of the $CO_2$ molecules was modeled by density functional theory calculations. The adsorption and separation of mixtures of *o*-, *m*-, and *p*-xylene from mesitylene showed a preferred adsorption of *o*-xylene. The structures of *o*/*m*/*p*-xylene-loaded CAU-13 were determined from PXRD data. The adsorption of xylene isomers induces a larger pore opening than that in the thermal activation of CAU-13. In the crystal structure of the activated sample CAU-13(empty pore), half of the linkers adopt the a,a confirmation and the other half the e,e conformation, and the presence of a,a-$CDC^{2-}$ ions hampers the structural flexibility of CAU-13. However, after the adsorption of xylene, all linkers are present in the e,e conformation, allowing for a wider pore opening by this new type of "breathing".

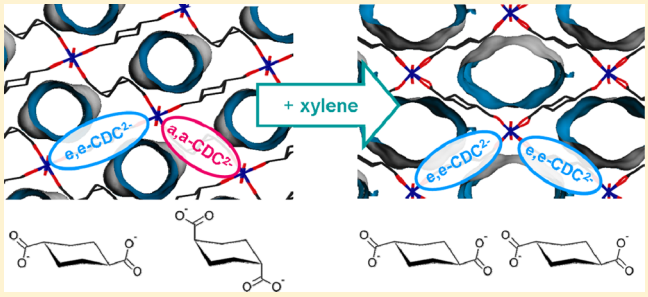


## INTRODUCTION

Owing to their potential applications in gas storage and separation, catalysis, and drug delivery or as sensor materials, metal−organic frameworks (MOFs) have become an important class of inorganic−organic hybrid materials.[1,2] These materials are often (micro)porous and are built up from inorganic building units such as metal ions or metal−oxygen clusters, which are linked by polydentate organic molecules. The great diversity of possible combinations of linkers with different inorganic building units allows the formation of a large variety of structures. Special interest lies in the investigation of MOFs that undergo structural transformations upon temperature and applied mechanical pressure changes or the inclusion of guest molecules. This unusual behavior of crystalline solids, described as "breathing", was discovered in 2002 for $[Co(NCS)_2(3\text{-PIA})_2]\cdot$guest [PIA = *N*-(3-pyridyl)isonicotinamide],[3] $[V^{III}(OH)BDC]\cdot$guest,[4] and [Cr(OH)BDC]·guest (BDC = 1,4-benzenedicarboxylate).[5] The latter examples represent the first MOFs with MIL-53-type structure, which have the general composition $[M^{III}(OH)BDC]\cdot$guest and which have now been studied in various functionalized forms. They are built up of zigzag chains of trans-corner-sharing $MO_6$ octahedra, with $M^{3+}$ being $Al^{3+}$, $Sc^{3+}$, $Cr^{3+}$, $Fe^{3+}$, $Ga^{3+}$, and $In^{3+}$.[4−10] The one-dimensional inorganic building units are interconnected via $BDC^{2-}$ ions, forming a network with diamond-shaped channels.

**Received:** February 5, 2014
**Published:** April 10, 2014

   dx.doi.org/10.1021/ic500288w | *Inorg. Chem.* 2014, 53, 4610−4620

When MIL-53 is stored at ambient conditions, it adsorbs water, leading to the so-called narrow-pore (np) form of the structure. When water is removed, for most of the MIL-53 compounds, a drastic increase of the unit cell volume occurs and the large-pore (lp) form of the structure is observed.[5] For Al-MIL-53, the unit cell volume changes by 33% upon dehydration.[11] The overall expansion or shrinkage of the framework of MOFs is often accompanied by a rotation of the organic and inorganic building units around a part of the structure that plays the role of a "knee-cap". In MIL-53, this is the axis through the carboxylate oxygen atoms.[12] Layered structures that are connected by flexible (aliphatic) pillar molecules can also exhibit a breathing effect,[13] which has, for example, been realized by layered zirconium phosphates pillared by alkyl diphosphonates.[14] General descriptions of the concept of breathing in inorganic–organic hybrid materials are given in review papers by Kitagawa et al. and Férey et al.[12,13,15] The breathing behavior of MIL-53 has been investigated by combining several experimental approaches including in situ powder X-ray diffraction (PXRD) during solvent exchange or exposure to various gases and vapors, infrared and micro-calorimetry measurements, and molecular simulations.[16−18] Concerning practical applications, an understanding of the adsorption of $CO_2$[19−22] and the separation of C8 alkyl aromatics (xylenes, ethylbenzene, etc.) is relevant.[23−25]

Recently, some of us have reported on the Al-MOF denoted as CAU-13 ([Al(OH)CDC]·guest), which is isoreticular to MIL-53 but contains the flexible aliphatic linker *trans*-1,4-cyclohexanedicarboxylate ($CDC^{2-}$).[26] *trans*-1,4-Cyclohexanedicarboxylic acid is able to undergo conformational changes in solution, leading to an equilibrium between the e,e and a,a conformers. Both conformers are present in the structure of CAU-13, and the same conformers are situated on opposing sides of the pore walls. The structures of MIL-53 and CAU-13 are compared in Figure 1. MIL-53 exhibits "smooth" pore walls, whereas the kinked a,a-$CDC^{2-}$ ions protrude into the channels of CAU-13.

Here, we present a comprehensive study on the sorption properties and framework flexibility of CAU-13 combining in situ and ex situ PXRD, molecular modeling based on density functional theory (DFT), and force-field-based calculations as well as high-pressure adsorption experiments. The adsorption of xylene isomers gave rise to a new manner of pore-size variation upon adsorption of guest molecules, which is accompanied by a conformational change of the cyclic aliphatic linker.

## EXPERIMENTAL SECTION

**Synthesis.** All reagents and solvents were purchased from commercial sources and used without further purification. Aluminum chloride hexahydrate ($AlCl_3·6H_2O$; puriss.) and *N*,*N*-dimethylformamide (DMF; 99.5%) were purchased from Grüssing GmbH, Filsum, Germany. *trans*-1,4-Cyclohexanedicarboxylic acid (*trans*-$H_2CDC$; 99%) was purchased from TCI Deutschland GmbH, Eschborn, Germany. The synthesis of CAU-13 was carried out as described in the literature using microwave-assisted heating.[26] Typically, 516 mg (3.00 mmol) of *trans*-$H_2CDC$ and 724 mg (3.00 mmol) of $AlCl_3·6H_2O$ were combined in a Biotage 10−20 mL glass reactor, and 16.0 mL of DMF and 4.00 mL of water were added. The reactor was sealed with a septum. The reaction mixture was heated in a Biotage Initiator microwave oven for 45 min at 130 °C under stirring. Product recovery was performed by centrifugation. The crude product was purified by stepwise treatment with DMF and ethanol for 45 min at 130 °C using the microwave oven. The compound was shown to also be stable in water upon treatment at the same conditions. Product purity and preservation of crystallinity were confirmed by PXRD.

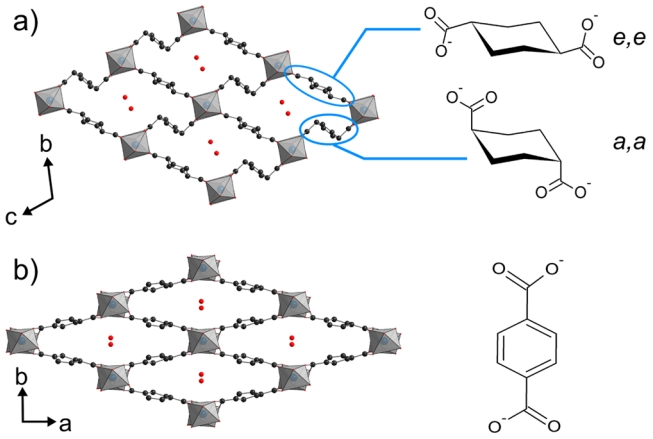


**Figure 1.** Ball-and-stick representations of the crystal structures and structural formula of the incorporated linkers of (a) CAU-13·$H_2O$ ([Al(OH)CDC]·$H_2O$) and (b) Al-MIL-53(np) ([Al(OH)BDC]·$H_2O$). $AlO_6$ polyhedra are presented as gray octahedra, carbon atoms as black spheres, and oxygen atoms (of adsorbed water molecules) as red spheres. Hydrogen atoms are omitted. The structures were drawn using the crystallographic data of ref 26 for part a and ref 11 for part b. On the right, the linkers present in the structures of CAU-13 and MIL-53 are shown: (a) e,e-$CDC^{2-}$ and a,a-$CDC^{2-}$; (b) $BDC^{2-}$.

**PXRD.** PXRD experiments for product identification were carried out on a Stoe Stadi P diffractometer in transmission geometry with Cu $K\alpha_1$ radiation, equipped with an image-plate detector system. The high-resolution PXRD pattern of activated CAU-13 for structure refinement was obtained at beamline P08 at PETRA III, DESY, Hamburg, Germany. The sample was prepared as follows: The purified and dried sample was filled into a borosilicate capillary (diameter: 0.7 mm), which was attached to a glass valve. The capillary was heated and evacuated (200 °C, $2 \times 10^{-3}$ kPa). After 2 h, the capillary was sealed. The PXRD patterns of CAU-13 loaded with *o*-, *m*-, and *p*-xylene were recorded on a PANalytical Empyrean diffractometer (Cu $K_{\alpha_1/\alpha_2}$ radiation) using a PIXcel3D detector. Amounts of 30 mgworking with TOPAS of the purified CAU-13 were placed in a DURAN Pyrex tube and mixed with 3 mL of *o*-, *m*-, or *p*-xylene. The mixture was heated at 100 °C for 5 h under stirring. After cooling to room temperature, the mixture was centrifuged and the supernatant was removed. The suspension was transferred into a glass capillary (diameter: 0.5 mm). The capillary was then centrifuged to concentrate the solid. Temperature-dependent PXRD measurements were recorded under air using a PANalytical Empyrean diffractometer equipped with an oven (TC-radiation, MRI) and a PIXcel3D detector. The samples were loaded into $Al_2O_3$ sample holders, and the patterns were recorded in reflection geometry with Cu $K_{\alpha_1/\alpha_2}$ radiation every 10 °C, heating the sample from 30 to 200 °C, then cooling it to 30 °C, and heating it again to 500 °C.

## INVESTIGATION OF THE BREATHING BEHAVIOR OF CAU-13 BY PXRD

**Thermal Treatment.** To quantify the changes in the unit cell parameters upon thermal treatment, Pawley refinements were carried out using each of the recorded PXRD patterns between 30 and 350 °C. The method of parametric Rietveld refinement, as implemented in the computer program *Powder 3D Parametric* by Rajiv et al.[27] working with *TOPAS-Academic*,[28] was applied. Because no obvious reconstructive transitions were observed, the number of phases was set to one. As starting values, the cell parameters of CAU-13·$H_2O$ were


dx.doi.org/10.1021/ic500288w | Inorg. Chem. 2014, 53, 4610−4620

Table 1. Details of the Rietveld Refinements of CAU-13(empty pore), CAU-13(*m*X), CAU-13(*o*X), and CAU-13(*p*X) Compared to the Unit Cell Parameters of CAU-13·$H_2O$

| | CAU-13(empty pore) | CAU-13(*m*X) | CAU-13(*o*X) | CAU-13(*p*X) | CAU-13·$H_2O$[a] |
|---|---|---|---|---|---|
| wavelength | 0.825986 (synchrotron radiation) | Cu $K_{\alpha_1/\alpha_2}$ | Cu $K_{\alpha_1/\alpha_2}$ | Cu $K_{\alpha_1/\alpha_2}$ | |
| space group | $P\bar{1}$ | $P2_1$ | $P2_1$ | $P2_1$ | $P\bar{1}$ |
| $a$/Å | 6.6237(3) | 6.6103(3) | 6.6031(8) | 13.225(2) | 6.6169(5) |
| $b$/Å | 9.7034(5) | 17.8984(9) | 18.060(2) | 17.892(2) | 9.4300(6) |
| $c$/Å | 9.4227(3) | 11.0989(5) | 10.858(7) | 11.0836(9) | 9.4642(6) |
| $\alpha$/deg | 108.362(2) | 90 | 90 | 90 | 107.577(3) |
| $\beta$/deg | 107.395(5) | 91.246(4) | 90.374(9) | 89.80(2) | 107.725(7) |
| $\gamma$/deg | 93.685(3) | 90 | 90 | 90 | 93.209(5) |
| $V$/Å$^3$ | 540.04(4) | 1312.8(1) | 1294.8(2) | 2622.6(5) | 529.08(7) |
| $Z$ | 2 | 4 | 4 | 8 | 2 |
| $R_{Bragg}$ | 0.93 | 0.44 | 0.68 | 0.38 | |
| $R_{wp}$ | 4.65 | 2.98 | 3.50 | 3.66 | |
| GOF | 0.89 | 1.72 | 2.28 | 2.46 | |

[a]The cell parameters of CAU-13·$H_2O$ were taken from ref 26.

chosen and refined to the first recorded PXRD pattern. The refined cell parameters are listed in Table S1 in the Supporting Information (SI).

**$CO_2$ Sorption.** The in situ PXRD (synchrotron radiation, $\lambda$ = 1.5406 Å) study during $CO_2$ adsorption at 195 K was performed at beamline KMC-2 at BESSY, Berlin, Germany. The experimental setup employing a BELSORP-max apparatus and a homemade sample holder is described elsewhere.[29] PXRD patterns were recorded at 16 points of the adsorption branch and 6 points of the desorption branch of the isotherm. The adsorption isotherm is presented in Figure S3 in the SI, together with an overview of the $CO_2$ pressures at which the PXRD patterns were recorded. To quantify the changes of the unit cell parameters, Pawley refinements were carried out using each of the recorded PXRD patterns by the method of parametric Rietveld refinement, as implemented in the computer program *Powder 3D Parametric*.[27] The number of observed phases was set to one. As starting values, the cell parameters of CAU-13(empty pore) were chosen because the sample had been thermally activated. The refined cell parameters are visualized in Figure S4 in the SI and listed in Table S2 in the SI. To localize the pressure-dependent positions of the $CO_2$ molecules in the framework of CAU-13, DFT calculations were carried out. For the calculations, a structure model of CAU-13 present upon $CO_2$ adsorption was built, starting with the crystal structure of CAU-13(empty pore) and fixing the unit cell parameters to the ones provided in Table S2 in the SI at a $CO_2$ pressure of 96.307 kPa using the same force-field-based computationally assisted structure determination as that described below [structure determination of CAU-13(xylene)]. The structural models were further geometry-optimized by DFT calculations in the absence and presence of one and two $CO_2$ molecules per unit cell. In a manner similar to that in our previous investigation on Al-MIL-53,[19] several starting configurations were considered for $CO_2$ in order to probe the possible geometries of this guest in the pores. These configurations include single interactions between $CO_2$ and either the OH groups of the inorganic structure parts or the organic linker and double interactions in which the guest molecule bridges two OH groups of opposing pore walls. Geometry optimization was performed with the PW91 GGA density functional[30] and the double numerical basis set containing polarization functions[31] on the hydrogen atom, as implemented in the Dmol$^3$ code.[29] The adsorption enthalpies were then calculated following the same method that we fully described in ref 21 to allow a direct comparison with the microcalorimetry measurements.

**Xylene Vapor-Phase Adsorption.** PXRD was used to examine the flexible behavior of CAU-13 in response to xylene vapor. A Bruker D8 diffractometer operating with Cu $K_{\alpha_1/\alpha_2}$ radiation was used for these experiments, with the hydrated sample packed into a ceramic holder and data measured in $\theta-\theta$ geometry using a VANTEC solid-state detector, which permitted a typical diffraction pattern to be accumulated in around 3 min. The diffractometer was equipped with an Anton Paar XRK 900 reactor chamber, which allowed accurate temperature control and for gases to be passed over the sample. For the adsorption experiments, nitrogen was bubbled through the chosen xylene isomer in a Drechsel bottle to introduce a vapor of xylene over the sample. The powdered sample was packed into the holder to allow space for expansion, and its height was checked after the experiment to ensure that no movement had occurred. The desorption of each xylene isomer was investigated by heating the xylene-loaded samples in air in the range 60−150 °C. Scans were recorded every 1 °C.

## STRUCTURE DETERMINATION

**CAU-13(empty pore).** The crystal structure of desolvated CAU-13 denoted as CAU-13(empty pore) was solved and refined from PXRD data obtained at beamline P08, PETRA III at DESY, Hamburg, Germany ($\lambda$ = 0.825986 Å). The sample was measured in a borosilicate glass capillary (diameter: 0.7 mm) after thermal activation. The experimental setup of the beamline is described in ref 32. After indexing the powder pattern and refining the cell parameters using *TOPAS-Academic*,[28] the structure was solved by direct methods in the space group $P\bar{1}$ using the program *EXPO 2009*.[33] With the extracted atomic positions set as the structural starting model, a Rietveld refinement using *TOPAS-Academic* was carried out. The profile was fitted using a Thompson−Cox−Hastings pseudo-Voigt profile function and a simple axial model. Soft distance restraints were applied to the C−C bonds of the organic linker molecule (C2−C3, C2−C4, C3−C4, C5−C6, C6−C7, C6−C8, and C7−C8). The Rietveld plot, an image of the asymmetric unit, and a table showing selected bond lengths are presented in the SI (Figures S6 and S7 and Table S3). The


dx.doi.org/10.1021/ic500288w | Inorg. Chem. 2014, 53, 4610−4620

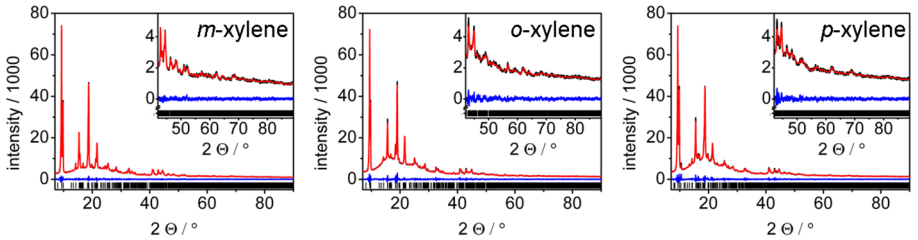


**Figure 2.** Final Rietveld plots of the structure refinements of CAU-13 loaded with xylene isomers (Cu $K_{\alpha_1/\alpha_2}$ radiation). The observed powder patterns are shown in black, the calculated powder patterns as an overlay in red, and the difference plots (observed − calculated) in blue. The tics mark the allowed Bragg peak positions.

unit cell parameters of CAU-13(empty pore) are listed in Table 1.

**CAU-13(xylene).** The PXRD patterns of CAU-13 loaded with an excess of liquid xylene of each isomer were recorded with Cu $K_{\alpha_1/\alpha_2}$ radiation on a PANalytical Empyrean diffractometer. The patterns were indexed with the program *EXPO 2009*,[33] and the unit cell parameters were refined with the Pawley method using *TOPAS-Academic*.[28] A Split Pearson VII profile function and a simple axial model were used for profile fitting. The Pawley fits are presented in Figure S8 in the SI, and the details of the refinements are listed in Table S4 in the SI.

A structural model was constructed starting from the crystal structure of the large-pore Al-MIL-53(lp) (space group *Imma*).[11] Using the program *Powdercell*,[34] the original orthorhombic crystal structure was converted subsequently into hypothetical ones with lower symmetry, using subgroups of *Imma* (sequence $Imma{-}I2_12_12_1{-}P2_12_12_1{-}P2_1$). The model of lowest symmetry was used as a starting point for constructing the structural model for CAU-13(*o*X) and CAU-13(*m*X) using the same computationally assisted structure determination strategy that some of us previously validated on different MOFs.[19,35] For that purpose, we considered the initial atomic positions of the large-pore form of Al-MIL-53 converted to the space group $P2_1$, the bonding scheme of the organic linker was changed from aromatic to aliphatic single bonds, and the unit cell parameters were changed to the respective indexed ones for CAU-13(*o*X) and CAU-13(*m*X). The obtained models were then geometry-optimized with fixed unit cell parameters using the generic universal force field,[36] as implemented in the *Forcite* software.[37] The indexing of the PXRD pattern of CAU-13(*p*X) resulted in a doubling of the length of the *a* axis compared to those of CAU-13(*o*X) and CAU-13(*m*X). The structural model for CAU-13(*p*X) was therefore obtained by doubling the *a* axis using again the supergroup−subgroup relation employed in *Powdercell*, and the same geometry optimization procedure as that described above was applied. Two *o*X and *m*X molecules as well as four *p*X molecules per unit cell were then introduced in the structure models. Their positions were energy-minimized by force-field-based simulations. Starting with the resulting structural models, Rietveld refinements were carried out using *TOPAS-Academic*.[28] The organic linker and xylene molecules were defined as rigid bodies, while the inorganic parts of the framework were freely refined. Because the guest molecules inside the channels arranged in close proximity to each other for the compounds adsorbing *o*- and *m*-xylene, their occupancies were constrained to reasonable values, indicating a disordered arrangement inside the channels after the refinements had converged. In the case of *p*-xylene, the guest molecules occupy well-defined positions. This leads to the doubled value for the *a* axis, which indicates a fully ordered arrangement of the guest molecules. For all structures, the refinements converged to reasonable figure-of-merit values. The details of the refinements are given in Table 1, and the final Rietveld plots are shown in Figure 2.

Figures of the asymmetric units as well as tables of selected atomic distances are given in the SI (Tables S5−S7 and Figures S9−S11).

## SORPTION EXPERIMENTS

**Sorption Isotherms.** Before the gas sorption experiments were performed, the powdered samples were thermally activated at 200 °C under vacuum for at least 2 h. However, the xylene vapor-phase adsorption experiments were carried out using the hydrated CAU-13·$H_2O$. Sorption experiments up to 1 bar were performed with a BELSORP-max apparatus (BEL Japan Inc.). The $N_2$ and $H_2$ sorption isotherms were recorded at 77 K, while the $CO_2$ and $H_2O$ sorption isotherms were recorded at 298 K. The apparent specific surface area was determined from the $N_2$ adsorption isotherm, as described in the literature.[38] The micropore volume was obtained at $p/p_0$ = 0.5. Calculations of the micropore volume were performed using the computer program *PLATON*[39] for the crystal structure of CAU-13(empty pore), with hydrogen atoms geometrically placed using *Materials Studio 5.0*.[37]

**Microcalorimetry.** Adsorption enthalpies were measured experimentally at 303 K and up to 40 bar using a Tian-Calvet type microcalorimeter coupled with an in-house manometric gas dosing system.[40−42] This apparatus allows the simultaneous measurement of the adsorption isotherm and the corresponding differential enthalpies. Gas is introduced into the system using a step-by-step method, and each dose is allowed to stabilize in a reference volume before being brought into contact with the adsorbent, located in the microcalorimeter. The introduction of the adsorbate to the sample is accompanied by an exothermic thermal signal, measured by the thermopiles of the microcalorimeter. The peak in the calorimetric signal is integrated over time to give the total energy released during that adsorption step.

**Xylene Liquid-Phase Adsorption.** Liquid-phase batch adsorption experiments were carried out according to a literature procedure.[23] A 1.8 mL vial with 25 mg of thermally activated CAU-13 and an empty reference vial were filled with a solution of one of the xylene isomers in mesitylene. The contents of the vials were stirred for 2 h at 298 K. Gas chromatography output data were used to determine the initial and equilibrium xylene concentrations. Adsorption isotherms were obtained by plotting the absorbed amount, in weight percentage, versus the equilibrium concentration. For competitive adsorption experiments, 0.2 mol $L^{-1}$ binary mixtures of


dx.doi.org/10.1021/ic500288w | Inorg. Chem. 2014, 53, 4610−4620

xylene isomers (0.1 mol $L^{-1}$ each) and a 0.3 mol $L^{-1}$ ternary mixture in mesitylene were used. Selectivities $\alpha_{i,j}$ were calculated using eq 1,

$$\alpha_{i,j} = \frac{q_i}{q_j}\frac{c_j}{c_i} \quad (1)$$

with $q_i$ and $q_j$ being the amounts (mol $g^{-1}$) of isomers $i$ and $j$ adsorbed per gram of MOF adsorbent, and $c_j$ and $c_i$ being the equilibrium concentrations (mol $L^{-1}$) of isomers $i$ and $j$ present in the liquid phase.

## RESULTS AND DISCUSSION

MIL-53-type compounds exhibit a large breathing effect upon adsorption and desorption of the guest molecules. For example, the pore diameter of Al-MIL-53·$H_2O$ increases drastically upon dehydration, whereas for Fe-MIL-53, an even narrower pore is observed.[43] On the other hand, different guest molecules also lead to various pore sizes.[16] To check whether CAU-13 shows a breathing effect, at first the structural changes were studied upon thermal dehydration. Furthermore, the influence of various gases and vapors on the structure of CAU-13 was studied.

**Thermal Behavior.** The thermal behavior of CAU-13·$H_2O$ was investigated with temperature-dependent PXRD measurements under air. To determine the framework flexibility, the sample was at first heated from 30 to 200 °C. The sample was then cooled to 30 °C and subsequently heated to 500 °C. PXRD patterns obtained at selected temperatures are shown in Figure 3 (top). The complete pattern series is presented in Figure S1 in the SI.

The temperature-dependent PXRD patterns show a reversible shift of some of the reflections' positions upon heating to 200 °C. In accordance with the previously published thermogravimetric data,[26] this effect can be attributed to the removal of water molecules from the channels. The reversibility of the observed phenomenon is attributed to the uptake of water from the air. Decomposition of the framework begins at around 350 °C. The structural changes were quantified by parametric refinement of the unit cell parameters. The plot of the cell lengths versus temperature presented in Figure 3 (bottom) shows that mainly the $b$ axis of the unit cell is influenced by the thermal treatment.

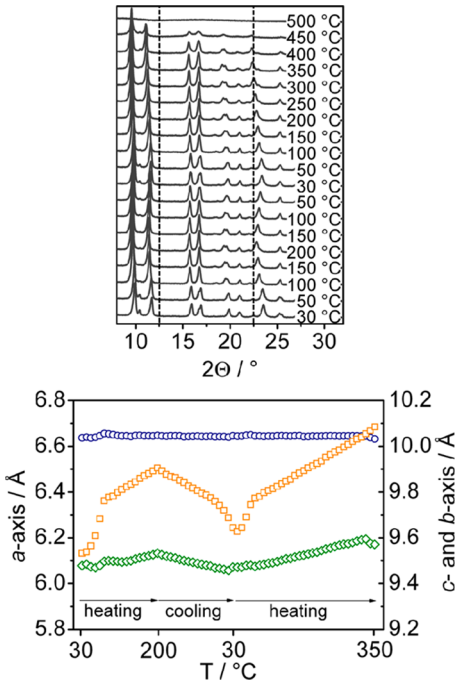


**Figure 3.** (Top) PXRD patterns of CAU-13 at selected temperatures (Cu $K_{\alpha_1/\alpha_2}$ radiation). The dashed lines at 12.5 and 22.5° ($2\theta$) are introduced to guide the eye. (Bottom) Evolution of the unit cell lengths over temperature: circles, $a$ axis; squares, $b$ axis; diamonds, $c$ axis.

The length of the $b$ axis increases upon the removal of adsorbed water up to 200 °C and then decreases during cooling. The reversibility of this effect could not be fully reached within the time frame of the experiment. However, the breathing effect is clearly observable. The finding that mainly the $b$ axis is affected shows that breathing occurs along the shorter intersection of the lozenge-shaped pores of CAU-13, thus causing a larger opening of the one-dimensional channels (Figure 1a). Small changes in the $c$ axis can be observed, whereas the length of the $a$ axis, which is parallel to the inorganic building unit (i.e., chains of trans-corner-sharing $AlO_6$ octahedra), remains almost unaltered. Similar observations can be made regarding the unit cell angles, whose progress with the temperature is presented in Figure S2 in the SI. The pore is further enlarged upon heating to temperatures higher than 200 °C due to thermal motion of the atoms.

On the basis of the temperature-dependent PXRD study, the crystal structure of CAU-13(empty pore) was determined using synchrotron PXRD data. CAU-13·$H_2O$ was transferred into a borosilicate glass capillary and thermally activated under vacuum. The structure was solved with direct methods and refined using the Rietveld method. CAU-13(empty pore) crystallizes in the space group $P\bar{1}$. Thus, no change of the space group could be observed for CAU-13 upon the removal/addition of water molecules. The main difference of the structures is the elongation of the $b$ axis in CAU-13(empty pore) due to the loss of hydrogen-bonding interactions connecting two inorganic building units via adsorbed water molecules. The desorption of water causes an increase of the unit cell volume of about 2% (Table 1). This breathing effect is very small compared to the 33% increase of the unit cell volume of Al-MIL-53 upon thermal activation.[11] The "kinked" a,a conformation of half of the $CDC^{2-}$ ligands in CAU-13 seems to prevent further pore opening.

**Sorption Properties.** Breathing may be triggered by guest molecules and observed as steps in the respective sorption isotherms because of the presence of different structures (and pore sizes) during the adsorption process. We investigated the sorption properties of CAU-13 towards various gases and vapors at low ($p \leq 1$ bar) and high pressures ($p \leq 40$ bar). From the adsorption isotherm of $N_2$ at 77 K, the specific surface area (380 $m^2$ $g^{-1}$) and the micropore volume (0.15 $cm^3$ $g^{-1}$) were determined. These experimental data are in good agreement with the calculated pore volume of 0.17 $cm^3$ $g^{-1}$ using *PLATON*[39] and the simulated accessible surface area (450 $m^2$ $g^{-1}$) estimated using a Monte Carlo algorithm, following the same strategy as previously reported by Düren et al.[44] The $H_2O$ sorption isotherm of CAU-13 at 298 K is presented in Figure 4, while the isotherms for $N_2$, $CO_2$, and $H_2$ obtained up to a pressure of 1 bar are shown in Figure S13 in the SI.

The $H_2O$ sorption isotherm exhibits an S shape. Because of the hydrophobic character of the pore walls, adsorption does


dx.doi.org/10.1021/ic500288w | Inorg. Chem. 2014, 53, 4610−4620

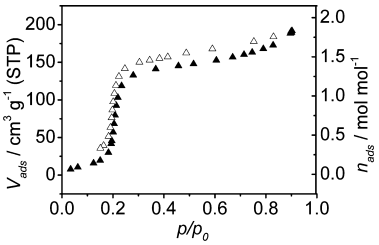


**Figure 4.** $H_2O$ sorption isotherm of CAU-13 recorded at 298 K.

not begin at low partial pressures but is shifted to $p/p_0$ = 0.15. This effect has also been observed for functionalized MIL-53 derivatives Al-MIL-53-Cl, -Br, and -$CH_3$.[45] The steep increase at $p/p_0$ = 0.2 corresponds to the adsorption of one water molecule per formula sum (Figure 4) and is in accordance with the water molecule that was localized in the structure of CAU-13·$H_2O$ by Rietveld refinement.[26] At higher relative pressures, a maximum of 1.8 mol mol$^{-1}$ water are adsorbed. The maximum amounts of $CO_2$ and $H_2$ adsorbed at 298 K and 1 bar are 75 and 6.8 mg g$^{-1}$, respectively. These values correspond to less than one molecule per formula sum (0.36 and 0.73 mol mol$^{-1}$). An overview of the adsorbed amounts in mol mol$^{-1}$, mg g$^{-1}$, and wt % is listed in the SI (Table S8). Except from the water sorption experiment, no stepwise adsorption of the guest molecules could be observed in the low-pressure region. In order to investigate whether such adsorption steps occur at higher adsorbate concentrations, high-pressure isotherms at 303 K were recorded using $N_2$, $CH_4$, $CO_2$, and CO. Simultaneously, the adsorption enthalpies were determined by microcalorimetry. The adsorption isotherms and a plot of the adsorption enthalpies against the adsorbed amount are reported in Figure 5. The exact adsorbed amounts and adsorption enthalpies are presented in Table S8 in the SI.

The high-pressure adsorption isotherms show that CAU-13 exhibits porosity towards all investigated gases. All isotherms show a steeper increase at lower pressures than at higher pressures, which is most distinct regarding the adsorption of $CO_2$ and $CH_4$. Unlike the MIL-53 compounds, CAU-13 does

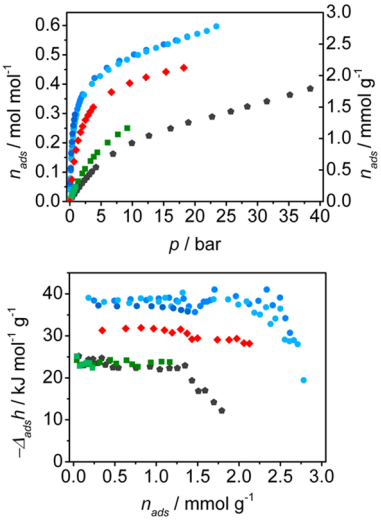


**Figure 5.** Adsorption isotherms (top) and enthalpies (bottom) for the adsorption of $N_2$ (gray pentagons), $CH_4$ (red diamonds), $CO_2$ (blue circles), and CO (green squares). Repetitions of one experiment are marked by symbols in different shades of the same color.

not show a stepwise adsorption of the investigated adsorbates, which implies that there are no guest-induced sudden structural changes. The observed capacities for the adsorbates are relatively small. At 303 K and 23 bar, CAU-13 adsorbs 2.78 mmol g$^{-1}$ $CO_2$ (0.60 mol mol$^{-1}$), similar to the amount adsorbed by the np form of Al-MIL-53, which is only stable up to a $CO_2$ pressure of 6 bar. However, the lp form of Al-MIL-53 is formed above this pressure and adsorbs almost 4 times the amount of $CO_2$ (~10 mmol g$^{-1}$, 2.1 mol mol$^{-1}$).[46] The relatively flat enthalpy profiles observed for all four samples during pore filling suggests a relatively homogeneous energetic surface. A comparison of the adsorption enthalpies obtained for the adsorption of $CO_2$ shows that the adsorption enthalpy of CAU-13 (−39 kJ mol$^{-1}$) is similar to that observed in the first step in the experiments with the np form of Al-MIL-53 (−35 kJ mol$^{-1}$)[46] or with STA-12 (−32 kJ mol$^{-1}$), which features open metal centers.[47] In contrast, the adsorption enthalpy for methane is remarkably higher for CAU-13 (−32 kJ mol$^{-1}$) compared to Al-MIL-53 (−17 kJ mol$^{-1}$).[46] Furthermore, the methane uptake is high with respect to that observed for nitrogen and carbon monoxide. This can be explained by the smaller pore diameter of CAU-13 and thus a higher degree of confinement, which leads to an increase of the host−guest interactions. However, these drastic differences in the methane adsorption enthalpies and uptakes of methane by CAU-13 may also be related to a contribution of the aliphatic pore environment.

**In Situ PXRD and $CO_2$ Adsorption.** The adsorption of water and $CO_2$ in MIL-53 leads to similar structural changes.[48] Because CAU-13 has already shown a small breathing effect upon the uptake of water, a similar effect was expected for the adsorption of $CO_2$. Because the adsorption isotherms measured at 298 and 303 K gave no direct evidence for a breathing effect, the $CO_2$ sorption of CAU-13 was additionally followed in situ by synchrotron PXRD at 195 K. At this lower temperature, a larger amount of $CO_2$ can be adsorbed. The experiments were performed at beamline KMC-2 at BESSY, Berlin, Germany. The corresponding adsorption isotherm is presented in Figure S3 in the SI (left) together with an overview of the relative pressures at which PXRD patterns were recorded. At the conditions used for this study (195 K, $p \leq 1$ bar), CAU-13 adsorbs 24 wt % (1.2 mol mol$^{-1}$) $CO_2$. During the experiment, PXRD patterns were recorded. Significant parts of the patterns are shown in Figure 6 (top). The full patterns are presented in Figure S3 (right) in the SI. A noticeable shift of the reflections corresponding to the crystallographic $b$ axis (i.e., 010 and 0$\bar{1}$1) can be observed, whereas the position of the 001 reflection is not remarkably influenced.

To gain deeper insight into the structural changes that underlie the observations, the unit cell parameters of CAU-13 were determined at various $CO_2$ loadings using parametric cell parameter refinement. In Figure 6 (bottom), evolution of the length of the $b$ axis over increasing partial pressure of $CO_2$ is presented together with the sorption isotherm.

Upon adsorption of about 0.5 $CO_2$ molecules per formula sum (CAU-13·0.5$CO_2$), i.e., one molecule per unit cell, the length of the $b$ axis reaches a minimum of 9.316(2) Å. This is even shorter than the length of the $b$ axis of CAU-13·$H_2O$ with 9.4300(6) Å. At higher pressures, the $b$ axis is elongated while more $CO_2$ is adsorbed, indicating a change in the interactions between $CO_2$ and the framework of CAU-13. For adsorption of the first $CO_2$ molecule per unit cell, the reduction of the pore opening suggests stronger host−guest interactions, whereas


dx.doi.org/10.1021/ic500288w | Inorg. Chem. 2014, 53, 4610−4620

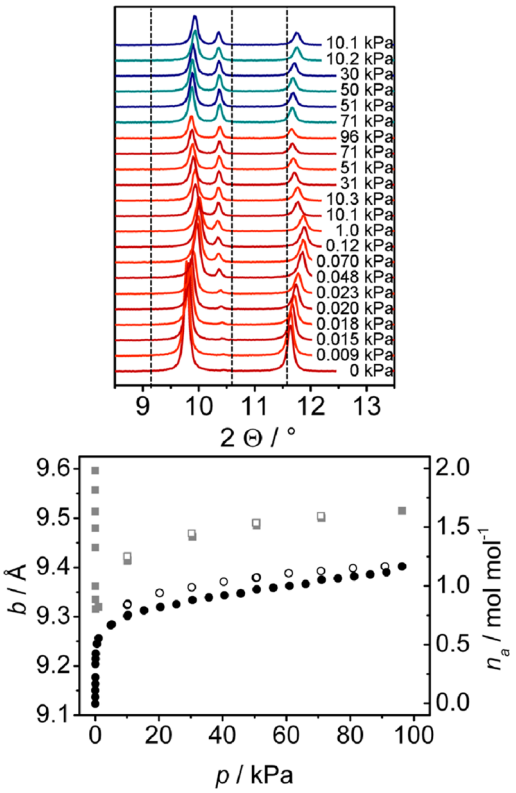


**Figure 6.** (Top) Synchrotron PXRD pattern series obtained during the adsorption (red patterns) and desorption (blue patterns) of $CO_2$. The PXRD patterns were measured using radiation with $\lambda$ = 1.5406 Å. From left to right, the 010, 001, and 0$\bar{1}$1 reflections are shown. The dashed lines were added to guide the eye. (Bottom) Evolution of the length of the crystallographic *b* axis with increasing pressure of $CO_2$ (squares). In addition, the corresponding $CO_2$ adsorption isotherm measured at 195 K (circles) is shown. Filled symbols mark the adsorption and open symbols the desorption.

upon the adsorption of more $CO_2$ molecules, the guest–guest interactions seem to dominate. The possible binding schemes were modeled by DFT calculations on the basis of the cell parameters observed at the partial pressures corresponding to the compositions of CAU-13·0.5$CO_2$ and CAU-13·$CO_2$, i.e., CAU-13 with one and two adsorbed $CO_2$ molecules per unit cell, respectively. The calculated arrangements of the $CO_2$ molecules inside the channels are shown in Figure 7.

The DFT calculations show that the presence of one $CO_2$ molecule per unit cell leads to a double interaction between the quadrupolar $CO_2$ and the OH groups of the framework via its $CO_2$ oxygen atoms. The end-on interaction of one $CO_2$ molecule with one OH group is found to be energetically less favorable. The characteristic $O_{CO_2}$–$H_{OH}$ distances of 2.78 and 2.82 Å between the $CO_2$ molecules and the framework OH groups are significantly longer than those we previously simulated for Al-MIL-53 at the same $CO_2$ concentration (2.07 and 2.10 Å).[18,19] This observation can be explained by the larger-pore aperture of CAU-13 (8.45 Å; see Figure S5 in the SI) compared to Al-MIL-53 in its narrow-pore form (6.78 Å). This results from the proximity of two $CDC^{2-}$ ions belonging to two neighboring chains, which prevents the pores from further closing and leads to a less confined environment for the guest molecules. These geometric considerations are consistent with a calculated adsorption enthalpy of −34 kJ $mol^{-1}$, which remains lower than the one previously simulated for $CO_2$ in Al-MIL-53 (−41 kJ $mol^{-1}$).[21] Nevertheless, the averaged experimentally observed adsorption enthalpy of Al-MIL-53 in the first adsorption step is −35 kJ $mol^{-1}$,[46] thus similar to both the experimental and calculated adsorption enthalpies of CAU-13.

When in the case of CAU-13·$CO_2$ two $CO_2$ molecules per unit cell are introduced (Figure 7, right), the binding scheme switches from the double interaction to an arrangement in which only one $CO_2$ oxygen atom is interacting with an OH group of the inorganic building unit. This is similar to previous findings for Al-MIL-53.[20,21] The calculated $O_{CO_2}$–$H_{OH}$ distances of 2.34 and 2.33 Å are shorter than that in the case of CAU-13·0.5$CO_2$, leading to a slightly higher adsorption enthalpy (−36 kJ $mol^{-1}$). The interactions between the $CO_2$ molecules lined up along the direction of the channel are relatively weak, represented by a characteristic $C_{CO_2}$–$C_{CO_2}$ distance of 3.76 Å.

Indeed, the differences in sorption behavior between Al-MIL-53 and CAU-13 are mainly based on the space the respective ligands occupy in the structure. This spatial arrangement influences the interactions between the $CO_2$ molecules and the framework. The interactions of $CO_2$ with CAU-13 and MIL-53

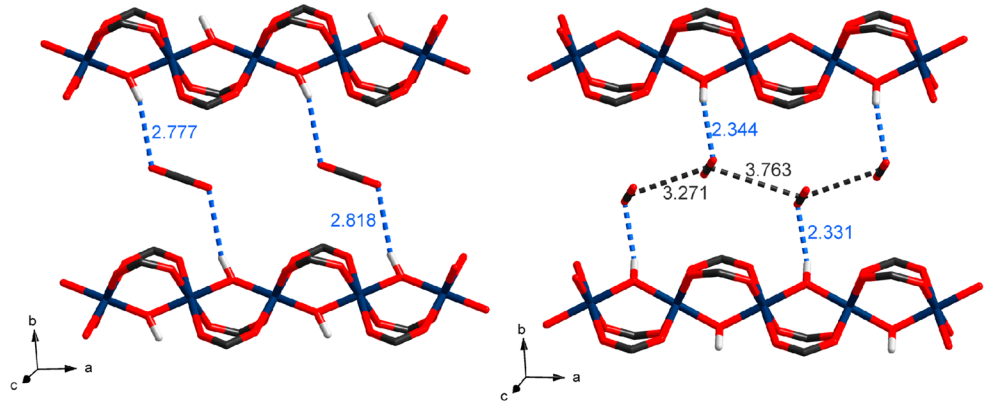


**Figure 7.** DFT-optimized arrangements of $CO_2$ in CAU-13: left, CAU-13·0.5$CO_2$; right, CAU-13·$CO_2$. The aliphatic cyclohexane rings are omitted for clarity. The characteristic interatomic distances are provided in angstroms. Color code: aluminum, blue; oxygen, red; carbon, black; hydrogen, light gray.


dx.doi.org/10.1021/ic500288w | Inorg. Chem. 2014, 53, 4610–4620

mainly occur between the adsorbate and the OH groups that are part of the inorganic building units.

## XYLENE ADSORPTION

So far, the steric properties of the aliphatic $CDC^{2-}$ ions dominated the sorption behavior of CAU-13. To study possible interactions with the aliphatic pore environment, xylene adsorption experiments were performed. In competitive adsorption experiments, the MIL-53 compounds showed a preference for *o*-xylene over the other isomers.[23,25] Crystal structure refinements of xylene-loaded Fe-MIL-53 indicated $\pi-\pi$ interactions not only between the adsorbate molecules but also between the adsorbate and the aromatic pore walls.[25] Because the pore walls of CAU-13 are aliphatic, such an interaction is improbable and should result in different sorption behavior.

We studied the liquid- and vapor-phase single-component xylene adsorption on CAU-13 and also the competitive adsorption from the liquid phase. In Figure 8, the liquid-phase batch adsorption isotherms of CAU-13 are presented. The experiments were carried out at 298 K using mesitylene as the eluent. For *o*-xylene, a slightly higher uptake (17 wt %, 0.34 mol $mol^{-1}$) than those for *p*-xylene (15 wt %, 0.29 mol $mol^{-1}$) and *m*-xylene (14 wt %, 0.28 mol $mol^{-1}$) can be observed.

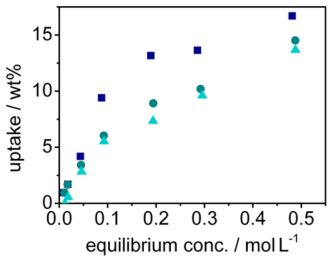


**Figure 8.** Liquid-phase batch adsorption isotherms of CAU-13 for *o*-xylene (squares), *p*-xylene (circles), and *m*-xylene (triangles) from mesitylene at 298 K.

In competitive adsorption experiments from a mixture of *o*- and *p*-xylene in hexane, the *o*-xylene uptake of Al-MIL-53 is higher (45 wt %, 0.88 mol $mol^{-1}$).[23] The selectivities given in Table 2 show only a slight preference of CAU-13 for *o*-xylene over the other isomers. While the separation factors of *o*/*m*-xylene and *o*/*p*-xylene are lower than those observed for Al-MIL-53, the separation of *m*/*p*-xylene results in similar selectivities (CAU-13:1.3, Al-MIL-53:1.2). This fact can be attributed to the shape-selective interactions of *o*-xylene in Al-MIL-53,[23] which are not possible in CAU-13.

**Table 2. Comparison of the Selectivities Calculated for the Adsorption from Equimolar Binary and Ternary Mixtures of Xylene Isomers by CAU-13 and Al-MIL-53**

| | $\alpha(o/p)$ | | $\alpha(o/m)$ | | $\alpha(p/m)$ | |
|---|---|---|---|---|---|---|
| mixture | CAU-13[a] | Al-MIL-53[b] | CAU-13[a] | Al-MIL-53[b] | CAU-13[a] | Al-MIL-53[b] |
| binary, *o*/*p* | 1.5 | 2.7 | | | | |
| binary, *o*/*m* | | | 1.9 | 3.5 | | |
| binary, *p*/*m* | | | | | 1.3 | 1.2 |
| ternary | 1.7 | | 2.1 | | 1.3 | |

[a]0.2 mol $L^{-1}$ binary or 0.3 mol $L^{-1}$ ternary mixtures in mesitylene. Batch experiments at 298 K. [b]0.028 mol mol $L^{-1}$ binary mixtures of xylene isomers in hexane. Batch experiments at 298 K. Experimental data from ref 23.

The lower capacity of CAU-13 is attributed to the smaller accessible pore volume due to the bulkier nature of the $CDC^{2-}$ ion in comparison to the $BDC^{2-}$ ion of Al-MIL-53. Not only does the aliphatic six ring of carbon atoms in the chair conformation need more space than the rigid planar aromatic ring of the $BDC^{2-}$ ions but also the number of hydrogen atoms has doubled. Because of the $sp^3$ configuration of the carbon atoms, the hydrogen atoms are not in the same plane as the carbon atoms but point in different directions. To find out if any structural changes occur when xylene is adsorbed, the vapor-phase adsorption of the xylene isomers was monitored by in situ PXRD. Figure 9 shows the contour maps of PXRD data collected during the adsorption as well as the desorption of xylene by CAU-13·$H_2O$. The adsorption experiments were performed using a steady flow of xylene-saturated nitrogen, and the PXRD patterns were recorded with a time resolution of ~3 min $scan^{-1}$. Desorption was achieved by stepwise heating.

Upon adsorption of the three different xylene isomers, structural changes of CAU-13 are observed. The beginning of the phase change is first seen for *m*-xylene (15 scans, approximately 45 min) followed by *o*-xylene (20 scans, approximately 60 min) and *p*-xylene (25 scans, approximately 75 min). During the adsorption of *o*- and *m*-xylene, the coexistence of two phases continues over a range of about 15–20 scans, while the phase change in the adsorption of *p*-xylene is faster (within less than 10 scans). The desorption experiments show that *p*-xylene is retained to the highest temperature followed by *o*- and *m*-xylene. Thus, only one step can be seen in each of the experiments with CAU-13, while Al-MIL-53 undergoes two steps in the adsorption of xylenes.[24] The observed phases during the adsorption are CAU-13·$H_2O$ in the beginning of the experiment and one phase for each of the xylene-loaded samples. During the desorption experiments, the resulting phase is CAU-13(empty pore) instead of CAU-13·$H_2O$ because desorption was achieved via thermal treatment. Interestingly, upon the adsorption of xylene, the reflections shift to lower angles, indicating an increase of the unit cell to values larger than those observed for CAU-13(empty pore) (Figure 10). To gain deeper insight into the structural changes triggered by the xylene adsorption of CAU-13, powdered samples were treated with an excess of the pure liquid xylene isomers and PXRD patterns were recorded. A comparison of the PXRD patterns of CAU-13·$H_2O$, CAU-13(empty pore), and CAU-13 loaded with xylene, collected during the in situ experiments and obtained with an excess of xylene, is shown in Figure 10.

The PXRD patterns exhibit a shift of the reflections to lower angles in the order CAU-13·$H_2O$ < CAU-13(empty pore) < CAU-13(xylene, vapor phase) < CAU-13(excess xylene). Indexing of the powder patterns obtained for CAU-13 loaded with the xylene isomers and Pawley refinements gave rise to cell volumes of 1350 $Å^3$ for the *m*-xylene-loaded sample and 1317 $Å^3$ for the *o*-xylene-loaded sample. The unit cell of *p*-xylene-containing CAU-13 is doubled in the direction of the one-dimensional pores (*a* axis), giving a cell volume of 2654 $Å^3$. The results of the refinement and final Pawley plots are presented in Table S4 and Figure S8 in the SI. With a cell content of $Z = 4$ [8 for CAU-13(*p*X)], this corresponds to a relative expansion by ~25% compared to CAU-13(empty pore) ($V = 540$ $Å^3$, $Z = 2$; Table 1). The volume changes are accompanied by an


dx.doi.org/10.1021/ic500288w | Inorg. Chem. 2014, 53, 4610–4620

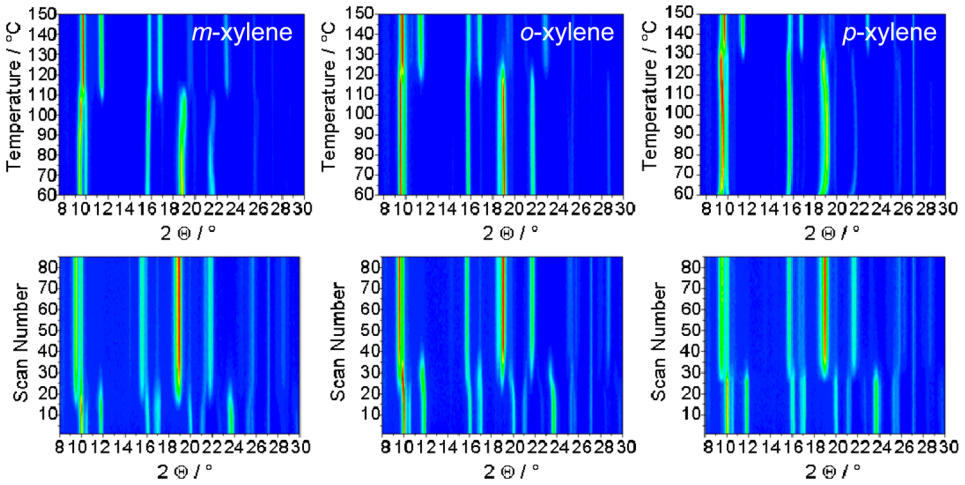


**Figure 9.** Contour maps of the in situ PXRD investigation of the adsorption (bottom) and desorption (top) of xylene isomers (Cu $K_{\alpha_1/\alpha_2}$ radiation). In the adsorption experiment, one scan number corresponds to approximately 3 min.

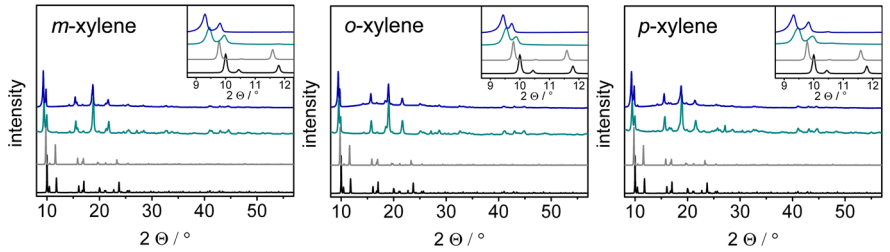


**Figure 10.** Comparison of the theoretical PXRD patterns of CAU-13·$H_2O$ (black) and CAU-13(empty pore) (gray) with the PXRD patterns of xylene-loaded samples: cyan, final pattern of vapor-phase adsorption experiments; blue, pattern of CAU-13 loaded with an excess of liquid xylene.

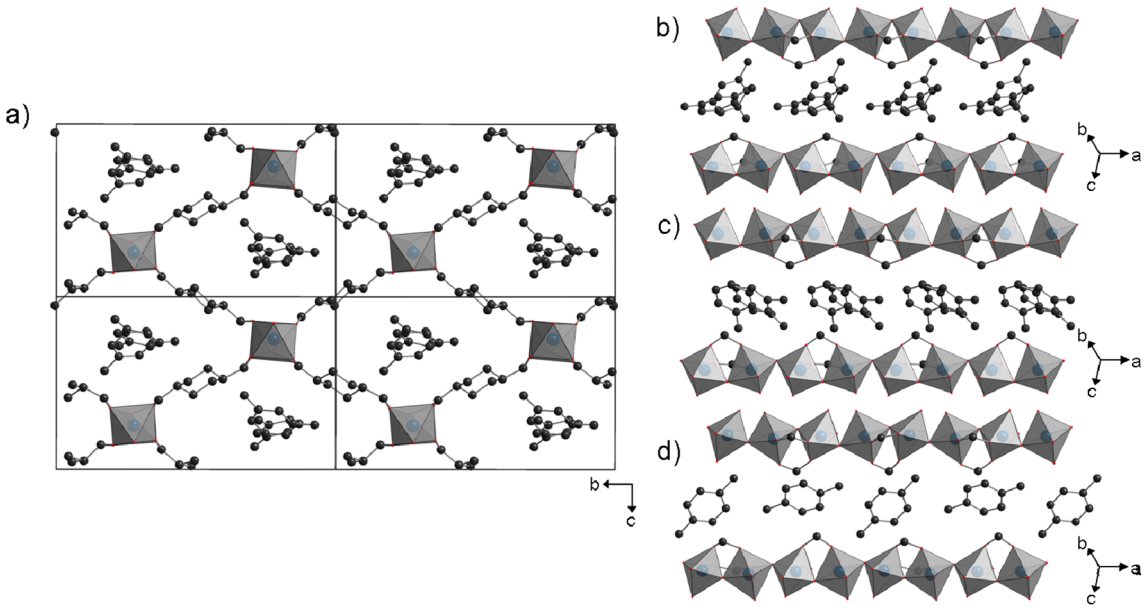


**Figure 11.** Ball-and-stick representations of the crystal structures of xylene-loaded CAU-13. (a) View along the channels of CAU-13(*m*X). Note the e,e conformation of all of the linker molecules. (b–d) Representative images of the arrangement of the xylene molecules in (b) CAU-13(*m*X), (c) CAU-13(*o*X), and (d) CAU-13(*p*X). In parts b–d, the carbon atoms of the cyclohexane rings are omitted for clarity.

increase of symmetry from the triclinic space group $P\bar{1}$ to the monoclinic space group $P2_1$. On the basis of these findings, structural models have been set up in the space group $P2_1$ using *Materials Studio 5.0*.[37] To allow for the large unit cell dimensions, all of the linker molecules had to be introduced using the e,e conformation, which represents the longer molecule of the two conformers [the $C_{carboxy}$–$C_{carboxy}$ distance of the e,e conformer is ~5.6 Å and that of the a,a conformer is ~4.6 Å, taken from the crystallographic data of CAU-13(empty pore)]. Rietveld refinements applying rigid bodies for both the linker and guest molecules proved the validity of the assumption. Representative images of the crystal structures of


dx.doi.org/10.1021/ic500288w | *Inorg. Chem.* 2014, 53, 4610–4620

the three xylene-loaded CAU-13 samples are given in Figures 11 and S12 in the SI.

As in CAU-13(empty pore), each chain of trans-corner-sharing $AlO_6$ octahedra is connected to four other chains by two types of crystallographically independent $CDC^{2-}$ ions; i.e., the topology of the structure is maintained. In the xylene-loaded CAU-13, both $CDC^{2-}$ ions are in the e,e conformation; however, in CAU-13(empty pore), half of the linker molecules are in the a,a- and e,e conformations, respectively. The pore aperture of CAU-13 is characterized by the Al−Al distance of two opposing inorganic building units and measures 9.70 Å for CAU-13(empty pore). The increase to around 11 Å determined for the xylene-loaded CAU-13 is only made possible by a conformational change of the flexible aliphatic linker molecules from the a,a conformation to the e,e conformation. In contrast, the breathing of MIL-53 is just accompanied by a rotation around the O−O axis of the O−M−M−O and O−C−O planes.[15] Breathing involving conformational changes of the flexible aliphatic linkers has so far only been reported for layers of zirconium phosphates pillared by aliphatic connectors such as 1,2-decanediphosphonates.[14] However, these layered compounds are of low crystallinity, and the pillaring connectors are statistically distributed throughout the layers, mixed with short monophosphonate molecules acting as space holders. Hence, the breathing of CAU-13 upon the adsorption of xylene represents a new kind of flexibility in MOFs.

The xylene molecules are located in the center of the pores in two different types of stacking. In CAU-13(*o*X) and CAU-13(*m*X), the positions of the xylene molecules are disordered, whereas in CAU-13(*p*X), an ordering of *p*-xylene can be observed. Therefore, the *a* axis of the unit cell of CAU-13(*p*X) is doubled compared to the structures of CAU-13(*o*X) and CAU-13(*m*X). The observed arrangements of the xylene molecules compare well with the behavior of the compound during the in situ PXRD experiments, where *p*-xylene is desorbed at the highest temperature followed by the other two isomers. The well-ordered array indicates relatively strong intermolecular adsorbate−adsorbate interactions, in good agreement with retention of the adsorbed molecules during the desorption experiment. The fact that only *p*-xylene is well ordered in CAU-13 might be due to its linear shape and its kinetic diameter, which is the smallest of the three isomers.

## CONCLUSION

The sorption properties and breathing behavior of the Al-MOF CAU-13 have been studied extensively and have been compared to those of Al-MIL-53. In summary, the adsorption capacities of CAU-13 are lower than those of Al-MIL-53, which adopts the *large-pore* form under similar experimental conditions. The micropore volume of CAU-13 is relatively small because of the bulkier aliphatic $CDC^{2-}$ ions in CAU-13 compared to the $BDC^{2-}$ ions in Al-MIL-53. A small breathing effect under thermal treatment in air (i.e., the desorption of water) and upon the adsorption of $CO_2$ was revealed. DFT calculations evidenced the most preferred arrangements of $CO_2$ within the pores of CAU-13 for different loadings, resulting in simulated adsorption enthalpies only slightly lower than those previously reported for Al-MIL-53, consistent with the microcalorimetry data. The adsorption of *o*-, *m*-, and *p*-xylene as single components and mixtures was investigated using solutions of the adsorbate in mesitylene. From mixtures in the liquid phase, *o*-xylene is adsorbed preferentially. The adsorption of the xylene isomers from the gas phase was monitored with in situ PXRD, which shows that upon desorption *p*-xylene is retained inside the pores to the highest temperature. Structure determinations of CAU-13 loaded with the xylene isomers reveal a remarkable breathing effect. The $CDC^{2-}$ ions that show the a,a and e,e conformations (ratio 1:1) in all other investigated forms of CAU-13 change their conformation upon loading with xylene to adopt the e,e conformation only. This results in a symmetry increase and allows for a wider pore opening and a cell volume increase by about 25%. This new type of breathing behavior has not been observed for any other MOF so far.

## ASSOCIATED CONTENT

### Supporting Information

X-ray crystallographic data in CIF format, details of the parametric refinement of the unit cell parameters for the temperature-dependent experiments as well as the in situ $CO_2$ sorption experiments (tabulated and graphical representations of the unit cell parameters, full PXRD patterns, and $CO_2$ sorption isotherms), images of the asymmetric units as well as bond length tables of CAU-13(empty pore), CAU-13(*m*X), CAU-13(*o*X), and CAU-13(*p*X), $N_2$, $CO_2$, and $H_2$ sorption isotherms recorded up to 1 bar, and a tabulated overview of all adsorbate uptakes of CAU-13 in the different experiments. This material is available free of charge via the Internet at http://pubs.acs.org. Crystallographic data for CAU-13(empty pore), CAU-13(*m*X), CAU-13(*o*X), and CAU-13(*p*X) have also been deposited with the Cambridge Crystallographic Data Centre (CCDC 980340, 980341, 980342, and 980343). The data can be obtained free of charge via the Internet at ww.ccdc.cam.a-c.uk/conts/retrieving.html or from the CCDC, 12 Union Road, Cambridge CB2 1EZ, U.K. (fax, +44 1223 36033; e-mail, deposit@ccdc.ac.uk).

## AUTHOR INFORMATION

### Corresponding Authors

*E-mail: guillaume.maurin@univ-montp2.fr.
*E-mail: stock@ac.uni-kiel.de. Tel.: +49-431-880-1675. Fax: +49-431-880-1775.

### Author Contributions

The manuscript was written through contributions of all authors. All authors have given approval to the final version of the manuscript.

### Notes

The authors declare no competing financial interest.

## ACKNOWLEDGMENTS

The research leading to these results has received funding from the European Community's Seventh Framework Programme (FP7MACADEMIA/2007-2013) under Grant 228862. D.d.V., J.L., and H.R. are grateful for support by IWT Belgium (MOFshape) and FWO (Vlaanderen). G.M. acknowledges the Institut Universitaire de France for financial support. A.H. and S.K. acknowledge the Federal Ministry of Education and Research for financial support (Project BMBF 05K10OD3). F.N. and N.S. are thankful for the support of the DFG (SPP 1362). We acknowledge the Helmholtz Association for beamtime on KMC-2 at BESSY and P08 at DESY.

## REFERENCES


(1) Themed issue on Metal-Organic Frameworks: *Chem. Soc. Rev.* **2009**, *38*, 1201−1508.
(2) Special Issue on Metal-Organic Frameworks: *Chem. Rev.* **2012**, *112*, 673−1268.
(3) Uemura, K.; Kitagawa, S.; Kondo, M.; Fukui, K.; Kitaura, R.; Chang, H.-C.; Mizutani, T. *Chem.—Eur. J.* **2002**, *8*, 3586−3600.
(4) Barthelet, K.; Marrot, J.; Riou, D.; Férey, G. *Angew. Chem., Int. Ed.* **2002**, *41*, 281−284.
(5) Serre, C.; Millange, F.; Thouvenot, C.; Noguès, M.; Marsolier, G.; Louër, D.; Férey, G. *J. Am. Chem. Soc.* **2002**, *124*, 13519−13526.
(6) Férey, G.; Latroche, M.; Serre, C.; Millange, F.; Loiseau, T.; Percheron-Guégan, A. *Chem. Commun.* **2003**, 2976−2977.
(7) Miller, S. R.; Wright, P. A.; Serre, C.; Loiseau, T.; Marrot, J.; Férey, G. *Chem. Commun.* **2005**, 3850−3852.
(8) Whitfield, T. R.; Wang, X.; Liu, L.; Jacobson, A. J. *Solid State Sci.* **2005**, *7*, 1096−1103.
(9) Volkringer, C.; Loiseau, T.; Guillou, N.; Férey, G.; Elkaim, E.; Vimont, A. *Dalton Trans.* **2009**, 2241−2249.
(10) Anokhina, E. V.; Vougo-Zanda, M.; Wang, X.; Jacobson, A. J. *J. Am. Chem. Soc.* **2005**, *127*, 15000−15001.
(11) Loiseau, T.; Serre, C.; Huguenard, C.; Fink, G.; Taulelle, F.; Henry, M.; Bataille, T.; Férey, G. *Chem.—Eur. J.* **2004**, *10*, 1373−1382.
(12) Férey, G. *Z. Anorg. Allg. Chem.* **2012**, *638*, 1897−1909.
(13) Kitagawa, S.; Uemura, K. *Chem. Soc. Rev.* **2005**, *34*, 109−119.
(14) Alberti, G.; Murcia-Mascarós, S.; Vivani, R. *J. Am. Chem. Soc.* **1998**, *120*, 9291−9295.
(15) Férey, G.; Serre, C. *Chem. Soc. Rev.* **2009**, *38*, 1380−1399.
(16) Millange, F.; Serre, C.; Guillou, N.; Férey, G.; Walton, R. I. *Angew. Chem., Int. Ed.* **2008**, *47*, 4100−4105.
(17) Walton, R. I.; Munn, A. S.; Guillou, N.; Millange, F. *Chem.—Eur. J.* **2011**, *17*, 7069−7079.
(18) Munn, A. S.; Ramirez-Cuesta, A. J.; Millange, F.; Walton, R. I. *Chem. Phys.* **2013**, *427*, 30−37.
(19) Devic, T.; Salles, F.; Bourrelly, S.; Moulin, B.; Maurin, G.; Horcajada, P.; Serre, C.; Vimont, A.; Lavalley, J.-C.; Leclerc, H.; Clet, G.; Daturi, M.; Llewellyn, P. L.; Filinchuk, Y.; Férey, G. *J. Mater. Chem.* **2012**, *22*, 10266−10273.
(20) Ramsahye, N. A.; Maurin, G.; Bourrelly, S.; Llewellyn, P. L.; Loiseau, T.; Serre, C.; Férey, G. *Chem. Commun.* **2007**, 3261−3263.
(21) Ramsahye, N. A.; Maurin, G.; Bourrelly, S.; Llewellyn, P. L.; Serre, C.; Loiseau, T.; Devic, T.; Férey, G. *J. Phys. Chem. C* **2008**, *112*, 514−520.
(22) Chen, L.; Mowat, J. P. S.; Fairen-Jimenez, D.; Morrison, C. A.; Thompson, S. P.; Wright, P. A.; Düren, T. *J. Am. Chem. Soc.* **2013**, *135*, 15763−15773.
(23) Alaerts, L.; Maes, M.; Giebeler, L.; Jacobs, P. A.; Martens, J. A.; Denayer, J. F. M.; Kirschhock, C. E. A.; De Vos, D. E. *J. Am. Chem. Soc.* **2008**, *130*, 14170−14178.
(24) Finsy, V.; Kirschhock, C. E. A.; Vedts, G.; Maes, M.; Alaerts, L.; De Vos, D. E.; Baron, G. V.; Denayer, J. F. M. *Chem.—Eur. J.* **2009**, *15*, 7724−7731.
(25) El Osta, R.; Carlin-Sinclair, A.; Guillou, N.; Walton, R. I.; Vermoortele, F.; Maes, M.; de Vos, D.; Millange, F. *Chem. Mater.* **2012**, *24*, 2781−2791.
(26) Niekiel, F.; Ackermann, M.; Guerrier, P.; Rothkirch, A.; Stock, N. *Inorg. Chem.* **2013**, *52*, 8699−8705.
(27) Rajiv, P.; Dinnebier, R. E.; Jansen, M. *Mater. Sci. Forum* **2010**, *651*, 97−104.
(28) Coelho, A. A. *TOPAS-Academic 4.1*; Coelho Software: Brisbane, Australia, 2007.
(29) Bon, V.; Senkovska, I.; Wallacher, D.; Heerwig, A.; Klein, N.; Zizak, I.; Feyerherm, R.; Dudzik, E.; Kaskel, S. *Microporous Mesoporous Mater.* **2014**, *188*, 190−195.
(30) Perdew, J. P.; Wang, Y. *Phys. Rev. B* **1992**, *45*, 13244−13249.
(31) Hehre, W. J.; Ditchfield, R.; Pople, J. A. *J. Chem. Phys.* **1972**, *56*, 2257−2262.
(32) Seeck, O. H.; Deiter, C.; Pflaum, K.; Bertam, F.; Beerlink, A.; Franz, H.; Horbach, J.; Schulte-Schrepping, H.; Murphy, B. M.; Greve, M.; Magnussen, O. *J. Synchrotron Radiat.* **2012**, *19*, 30−38.
(33) Altomare, A.; Camalli, M.; Cuocci, C.; Giacovazzo, C.; Moliterni, A.; Rizzi, R. *J. Appl. Crystallogr.* **2009**, *42*, 1197−1202.
(34) Kraus, W.; Nolze, G. *J. Appl. Crystallogr.* **1996**, *29*, 301−303.
(35) Devic, T.; Horcajada, P.; Serre, C.; Salles, F.; Maurin, G.; Moulin, B.; Heurtaux, D.; Clet, G.; Vimont, A.; Grenèche, J.-M.; Le Ouay, B.; Moreau, F.; Magnier, E.; Filinchuk, Y.; Marrot, J.; Lavalley, J.-C.; Daturi, M.; Férey, G. *J. Am. Chem. Soc.* **2010**, *132*, 1127−1136.
(36) Rappe, A. K.; Casewit, C. J.; Colwell, K. S.; Goddard, W. A.; Skiff, W. M. *J. Am. Chem. Soc.* **1992**, *114*, 10024−10035.
(37) *Materials Studio*, version 5.0; Accelrys Inc.: San Diego, CA, 2009.
(38) Rouquerol, J.; Llewellyn, P.; Rouquerol, F.; Rodriquez-Reinoso, F.; Seaton, N. *Stud. Surf. Sci. Catal.* **2007**, *160*, 49−56.
(39) Spek, A. L. *PLATON, A Multipurpose Crystallographic Tool*, version 1.16; Utrecht Universität: Utrecht, The Netherlands, 2011.
(40) Llewellyn, P. L.; Maurin, G. *C. R. Chim.* **2005**, *8*, 283−302.
(41) Llewellyn, P. L.; Bourrelly, S.; Serre, C.; Vimont, A.; Daturi, M.; Hamon, L.; De Weireld, G.; Chang, J.-S.; Hong, D.-Y.; Hwang, Y. K.; Jhung, S. H.; Férey, G. *Langmuir* **2008**, *24*, 7245−7250.
(42) Yang, Q.; Wiersum, A. D.; Jobic, H.; Guillerm, V.; Serre, C.; Llewellyn, P. L.; Maurin, G. *J. Phys. Chem. C* **2011**, *115*, 13768−13774.
(43) Millange, F.; Guillou, N.; Walton, R. I.; Grenèche, J.-M.; Margiolaki, I.; Férey, G. *Chem. Commun.* **2008**, 4732−4734.
(44) Düren, T.; Millange, F.; Férey, G.; Walton, K. S.; Snurr, R. Q. *J. Phys. Chem. C* **2007**, *111*, 15350−15356.
(45) Biswas, S.; Ahnfeldt, T.; Stock, N. *Inorg. Chem.* **2011**, *50*, 9518−9526.
(46) Bourrelly, S.; Llewellyn, P. L.; Serre, C.; Millange, F.; Loiseau, T.; Férey, G. *J. Am. Chem. Soc.* **2005**, *127*, 13519−13521.
(47) Miller, S. R.; Pearce, G. M.; Wright, P. A.; Bonino, F.; Chavan, S.; Bordiga, S.; Margiolaki, I.; Guillou, N.; Férey, G.; Bourrelly, S.; Llewellyn, P. L. *J. Am. Chem. Soc.* **2008**, *130*, 15967−15981.
(48) Serre, C.; Bourrelly, S.; Vimont, A.; Ramsahye, N. A.; Maurin, G.; Llewellyn, P. L.; Daturi, M.; Filinchuk, Y.; Leynaud, O.; Barnes, P.; Férey, G. *Adv. Mater. (Weinheim, Ger.)* **2007**, *19*, 2246−2251.